

Full Transformer Framework for Robust Point Cloud Registration with Deep Information Interaction

Guangyan Chen¹, Meiling Wang¹, Yufeng Yue^{1*}, Qingxiang Zhang¹, Li Yuan²
¹ Beijing Institute of Technology ² National University of Singapore

Abstract

Recent Transformer-based methods have achieved advanced performance in point cloud registration by utilizing advantages of the Transformer in order-invariance and modeling dependency to aggregate information. However, they still suffer from indistinct feature extraction, sensitivity to noise, and outliers. The reasons are: (1) the adoption of CNNs fails to model global relations due to their local receptive fields, resulting in extracted features susceptible to noise; (2) the shallow-wide architecture of Transformers and lack of positional encoding lead to indistinct feature extraction due to inefficient information interaction; (3) the omission of geometrical compatibility leads to inaccurate classification between inliers and outliers. To address above limitations, a novel full Transformer network for point cloud registration is proposed, named the Deep Interaction Transformer (DIT), which incorporates: (1) a Point Cloud Structure Extractor (PSE) to model global relations and retrieve structural information with Transformer encoders; (2) a deep-narrow Point Feature Transformer (PFT) to facilitate deep information interaction across two point clouds with positional encoding, such that Transformers can establish comprehensive associations and directly learn relative position between points; (3) a Geometric Matching-based Correspondence Confidence Evaluation (GMCCE) method to measure spatial consistency and estimate inlier confidence by designing the triangulated descriptor. Extensive experiments on clean, noisy, partially overlapping point cloud registration demonstrate that our method outperforms state-of-the-art methods. Code is publicly available at <https://github.com/CGuangyan-BIT/DIT>.

1. Introduction

Point cloud registration aims to calculate a rigid transformation to align two point clouds, which is a key technology for 3D reconstruction, simultaneous localization and mapping (SLAM) [14, 21]. In recent decades, point cloud registration has developed from model-based meth-

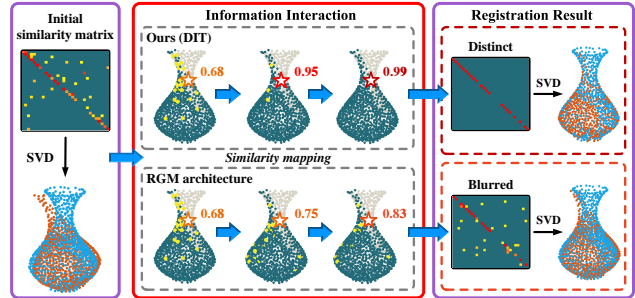


Figure 1. **The comparison between RGM [19] and our method (DIT) on partial-to-partial point cloud registration.** Through deep information interaction, DIT obtains higher values in the similarity mapping for queried points (\star). Therefore, DIT generates a more distinct similarity matrix by improving the discrimination of features, and ultimately improves registration accuracy.

ods [4, 5, 26, 43, 65], and convolutional neural network (CNN)-based methods [1, 12, 20, 64], to recent Transformer-based methods [19, 34, 48, 53]. These attempts have greatly increased the accuracy and robustness of point cloud registration by improving the defects of inefficient feature extraction and blurred mapping.

The most widely known model-based method is iterative closest point (ICP) [4], which iteratively alternates between establishing correspondences and calculating a transformation. However, ICP and its variants [10, 28, 35, 46, 47, 49] tend to converge to local minima due to the limited descriptive power of hand-crafted features. Recently proposed CNN-based methods are able to learn rich and general features compared with model-based methods. However, they only extract features from each point cloud separately and are consequently unable to extract discriminative features or identify common structures between two point clouds.

Attention-based models such as Transformer [50], which were first applied in natural language processing (NLP) [6, 15, 29], have also shown superior ability to extract features and aggregate information in computer vision tasks [9, 16, 24, 40, 51, 59, 60]. Inspired by the success of Transformers, recent works [19, 22, 48, 53, 54] investigated the advantages of Transformer models in point feature extraction. Most of them utilized the attention mechanism to es-

establish associations across two point clouds for information aggregation. However, substantial gaps remain in terms of modeling global relations, enhancing feature richness, and detecting inliers: (1) current methods mainly add attention modules to a CNN framework for information aggregation, leading to the sensitivity to noise; (2) the insufficient associations established by shallow-wide Transformers and lack of positional information prevent the model from enhancing feature richness and extracting distinct features; (3) the inlier detection modules did not consider spatial consistency of rigid transformations, resulting in low accuracy in removing outliers.

We argue that there is a key similarity between NLP and point cloud registration, namely, the need to establish associations between units representing the same content but with different expressions. Motivated by this observation and the limitations of previous Transformer-based methods, we propose a novel full Transformer framework named Deep Interaction Transformer (DIT), which takes advantage of the Transformer architecture to achieve global receptive field and deep information interaction. The process of deep information interaction is shown in Fig. 1, which improves the discrimination of features. Experimentally, the proposed method is compared with extensive registration methods, indicating that the proposed method achieves superior performance. The main contributions are four-fold:

- A Point Cloud Structure Extractor (PSE) is proposed to model global relations and integrate structural information. Concretely, Transformer encoders are adopted to model dependencies in the entire point cloud, enhancing the robustness to noise. In PSE, the Local Feature Integrator (LFI) is designed to structurize the point cloud, which addresses the limitation of Transformers in extracting structural features.
- A Point Feature Transformer (PFT) is proposed to increase the richness of feature representation. Specifically, deep-narrow Transformers are adopted to establish comprehensive associations. In PFT, a positional encoding network is introduced to allow the model to learn the relative position between points.
- A Geometric Matching-based Correspondence Confidence Evaluation (GMCCE) method is proposed to estimate the correspondence confidence based on geometric constraints. Specifically, a rotation-invariant triangulated descriptor is designed to measure geometrical compatibility.
- The proposed DIT is a systematic framework that implements above novel components to improve the robustness to noise and discrimination of features. The DIT achieves superior performance in accuracy and robustness compared with state-of-the-art methods.

2. Related Work

2.1. Model-Based Registration Methods

The most representative model-based method is the ICP algorithm [4], which iteratively alternates between finding the closest points as correspondences and calculating a transformation based on the identified correspondences. However, ICP and its variants [5, 37, 42, 46] often converge to local minima when the initial position is far from the global minimum. There is a large volume of works [7, 8, 17, 25, 33, 41, 56] that attempt to improve the robustness of ICP under poor initialization. In Gaussian mixture models (GMMs) [26], the registration problem is reformulated as the alignment of two probability distributions. However, these methods still require a warm initialization due to their nonconvex objective functions. In globally optimal ICP (Go-ICP) [57], the branch-and-bound (BnB) method is applied to search over $SE(3)$ space to achieve global convergence, but the computational complexity is much higher than that of ICP. Fast global registration (FGR) [65] relies on optimizing a global objective function to align two point clouds without any updating of correspondences. In addition, hand-crafted local features [43–45] such as fast point feature histograms (FPFH) are also designed to establish correspondences through feature matching. However, the accuracy and robustness of all of these model-based methods are sensitive to partially visible point clouds and large initial errors.

2.2. CNN-Based Registration Methods

The success of deep learning in point cloud processing [13, 36, 38, 39, 62] enables its application in point cloud registration. One pioneering work is PointNetLK (PNetLK) [1], which extracts global features using PointNet [38] and applies the inverse compositional Lucas-Kanade (IC-LK) algorithm [32] to align two point clouds. PointNetLK Revisited (PNetLK_R) [31] has been proposed to circumvent the numerical instabilities of PointNetLK using analytical Jacobians. However, since PointNet cannot aggregate the information from two point clouds, these two methods are sensitive to partially visible point clouds. Deep Gaussian mixture registration (DeepGMR) [61] relies on a neural network to predict the GMM parameters and recover the optimal transformation. However, due to the independence of the feature extraction from two point clouds, the features extracted by DeepGMR are indistinct. A robust point matching network (RPM-Net) [58] combines the Sinkhorn method with deep learning to establish soft correspondences from hybrid features, thereby enhancing the robustness to noise. In summary, these methods extract features from each point cloud separately and lack information interaction between the source and target point clouds, which is inefficient in discriminative feature extraction and

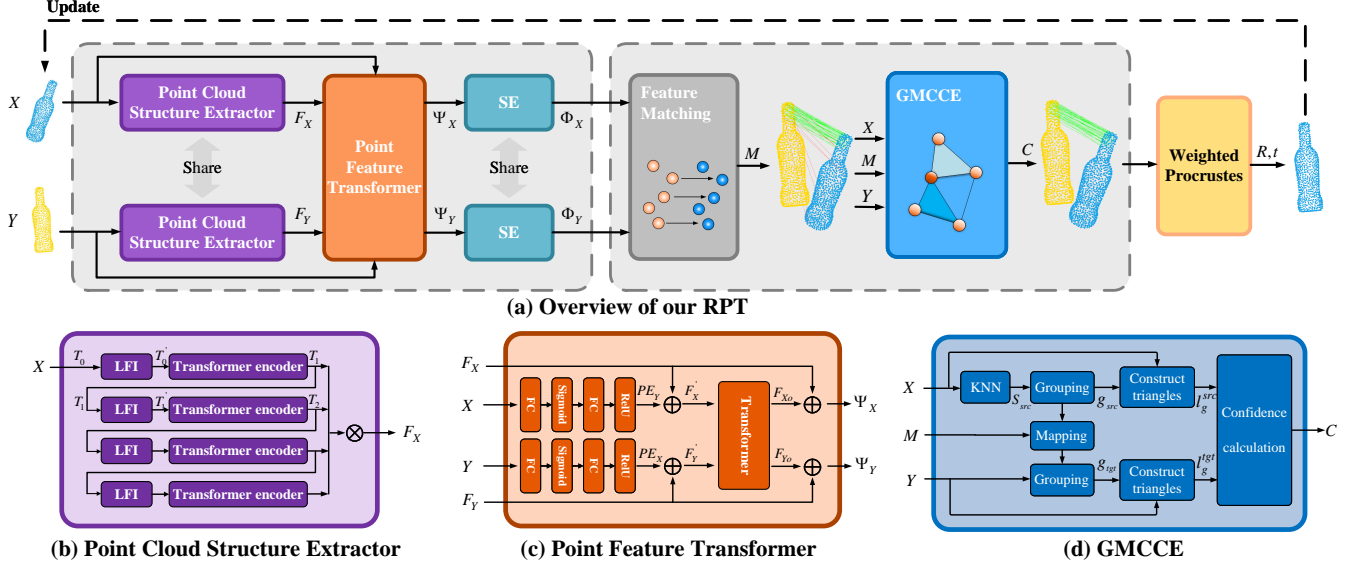


Figure 2. (a) Network architecture of the Deep Interaction Transformer (DIT). DIT consists of three main components: (b) Point Cloud Structure Extractor (PSE) and (c) Point Feature Transformer (PFT) to extract features, where \otimes denotes concatenation, \oplus denotes matrix addition; (d) Geometric Matching-based Correspondence Confidence Evaluation (GMCCE) module to evaluate correspondence confidence.

contextual information aggregation, especially in partial-to-partial point cloud registration tasks.

2.3. Transformer-Based Registration Methods

Inspired by the success of Transformers in NLP and computer vision, researchers have begun to apply Transformers to extract contextual information between two point clouds. Deep closest point (DCP) [53] extracts features using dynamic graph CNN (DGCNN) [36] and utilizes a Transformer [50] to aggregate information. However, DCP lacks an overall understanding of the point cloud due to its local receptive field, which leads to sensitivity to noise. A multiplex dynamic graph attention network (MDGAT) [48] dynamically constructs a multiplex graph based on an attention mechanism. A geometry guided network [34] encodes global and local features based on a self-attention mechanism with a fully connected graph. The recent robust graph matching (RGM) method [19] adopts a Transformer to aggregate information by generating soft graph edges. However, the edge adjacency matrices are indistinct due to the shallow-wide architecture of the Transformer, which leads to a decrease in registration accuracy. In summary, these methods mainly focus on modeling local relations by directly adopting convolution encoders, which prevents them from modeling global relations. Furthermore, the information interaction in these methods is inefficient due to the shallow-wide Transformer architecture and the lack of positional encoding.

3. The Proposed Deep Interaction Transformer

The point cloud registration problem aims to find a transformation to align two point clouds. Given two point clouds $X = \{x_1, x_2, \dots, x_N\} \subseteq R^3$ and $Y = \{y_1, y_2, \dots, y_M\} \subseteq R^3$, which are denoted by src and tgt , respectively, the objective is to estimate a rotation matrix $R \in SO(3)$ and a translation vector $t \in R^3$ to map src to tgt .

The overall pipeline of DIT is shown in Fig. 2(a). During training, the registration pipeline begins by extracting pointwise features F_X and F_Y from src and tgt separately using PSE. Then, deep information interaction is conducted by PFT to learn contextual information and extract discriminative features Φ_X and Φ_Y . These features are matched to establish putative correspondences $M\{x_i, y_j\}$. Finally, the weighted Procrustes module estimates the optimal transformation $\{R, t\}$ to align the two point clouds based on the established correspondences M and the similarity S between the corresponding feature vectors $\{\Phi_{x_i}, \Phi_{y_j}\}$. During testing, the GMCCE module is introduced to evaluate the correspondence confidence $C(x_i, y_j)$, and then the weighted Procrustes module estimates the optimal transformation based on the confidence $C(x_i, y_j)$ instead of the feature vector similarity.

3.1. Point Cloud Structure Extractor

Since the previous Transformer-based methods mainly employ features from CNN, which cannot model global relations. Therefore, the PSE module is designed to enhance the robustness to noise by modeling dependencies in the entire point cloud. Fig. 2(b) shows the PSE architecture,

which consists of two types of components: LFIs and Transformer encoders [2].

To overcome the limitation of Transformers in structural feature extraction [16,59], the LFIs are designed to progressively structurize the point cloud. As detailed in Fig. 3, to identify the characteristics of the neighboring structures, the n_{th} LFI ($n = 1, \dots, N_l$) searches for the local point cloud P_n that contains the k nearest points for each point in X , where N_l denotes the number of LFI layers. Specifically, the LFI applies the k -nearest neighbors (KNN) method in geometric space instead of feature space to reduce the computational expense. Then, the n_{th} LFI integrates structural information by concatenating (Concat) feature vectors $T_{P_n}^i$ of the points in P_n to construct integrated feature vectors T'_n :

$$T'_n = \text{Concat}([T_{P_n}^1, T_{P_n}^2, \dots, T_{P_n}^k]). \quad (1)$$

With the structural features T'_n , the Transformer encoder is adopted to model global relations in the point cloud [63]. Each Transformer encoder consists of a multilayer perceptron (MLP), layer normalization (LN), and the multi-head self-attention operation (MSA), which is based on multi-head attention (MA). MA is formulated as

$$\begin{aligned} \text{Att}(Q, K, V) &= \text{softmax}\left(\frac{QK^T}{\sqrt{d_K}}\right)V, \\ \text{MA}(F_Q, F_K, F_V) &= \text{Concat}(A_1, \dots, A_h)W^O, \end{aligned} \quad (2)$$

where $A_i = \text{Att}(F_Q W_i^Q, F_K W_i^K, F_V W_i^V)$; W_i^Q, W_i^K , and W_i^V are the projection matrices used to project F_Q, F_K , and F_V to queries Q , keys K , and values V ; h is the number of attention functions Att performed in parallel; d_K is the dimensionality of K ; W^O is a matrix used to project the concatenated features.

With regard to the MSA in the Transformer encoder, $\text{MSA}(T'_n) = \text{MA}(T'_n, T'_n, T'_n)$. MSA linearly projects T'_n onto Q, K , and V with different linear projections h times; then, each Att obtains an attention map by the scaled dot-product between Q and K to consider all relations between each point in src , and multiplies this map by V to aggregate information from the entire src . By conducting MSA and MLP, the encoder obtains T_{n+1} based on MLP and MSA as

$$\begin{aligned} \hat{T} &= \text{LN}(\text{MSA}(T'_n)) + T'_n, \\ T_{n+1} &= \text{LN}(\text{MLP}(\hat{T})) + \hat{T}. \end{aligned} \quad (3)$$

Finally, obtaining all output values T_n of Transformer encoders, with $n = 2, \dots, N_l + 1$, low-order and high-order features are merged by concatenating all features T_n as

$$F_X = \text{LN}(\text{ReLU}(\text{Concat}(T_2, T_3, \dots, T_{N_l+1}))). \quad (4)$$

3.2. Point Feature Transformer

The features F_X and F_Y extracted by PSE are still independent of each other, which leads to an indistinct similar-

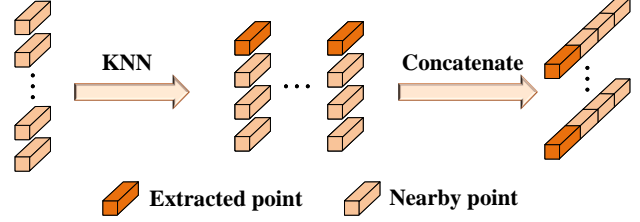


Figure 3. **Local Feature Integrator (LFI)**. KNN is applied to search for nearby points, then the feature vectors of nearby points and the extracted point are concatenated.

ity matrix. Therefore, to learn the contextual information of two point clouds and extract discriminative features, PFT is designed to facilitate deep information interaction.

Since the standard Transformer can not directly learn the relative position between points [50], positional encoding is introduced to extract positional information. To model the positional information P_X with coordinates X [63], an efficient neural network is introduced, which consists of fully connected layers FC, rectified linear unit ReLU activation, and sigmoid activation:

$$P_X = \text{ReLU}(\text{FC}(\text{Sigmoid}(\text{FC}(X)))). \quad (5)$$

Subsequently, we sum the positional information P_X and P_Y with the extracted features F_X and F_Y to obtain features F'_{Xa} and F'_{Ya} , respectively.

To aggregate information from src and tgt , a standard Transformer ϕ is adopted, which consists of an encoder (Eq. 3) and a decoder. The Transformer decoder consists of a multi-head cross-attention operation (MCA), in addition to MSA, MLP, and LN (Eq. 2). Taking $\phi(F'_Y, F'_X)$ as an example, the procedure is defined as

$$\begin{aligned} F_{Xa} &= \text{LN}(\text{MSA}(F'_X) + F'_X), \\ F'_{Xa} &= \text{LN}(\text{MCA}(F_{Ya}, F_{Xa}) + F_{Xa}), \\ F_{Xo} &= \text{LN}(\text{MLP}(F'_{Xa}) + F'_{Xa}), \end{aligned} \quad (6)$$

where $\text{MCA}(F_{Ya}, F_{Xa}) = \text{MA}(F_{Xa}, F_{Ya}, F_{Ya})$; features F_{Xa} are obtained based on MSA; features F_{Ya} are acquired through the encoder; the attention map is acquired in MCA to establish the associations across points in X and Y , which enables F_{Xa} to receive information from F_{Ya} and improves the discrimination of F_{Xa} .

However, due to the shallow-wide architecture used in previous methods, the associations established for information interaction are limited, leading to low feature richness. In this paper, we instead utilize a deep-narrow architecture to establish comprehensive associations.

Overall, the feature vectors Ψ_X and Ψ_Y generated by the Transformer are formulated as

$$\begin{aligned} \Psi_X &= F_X + \phi(F'_Y, F'_X), \\ \Psi_Y &= F_Y + \phi(F'_X, F'_Y). \end{aligned} \quad (7)$$

To adaptively recalibrate the channel-wise features in ac-

Algorithm 1 Correspondence Confidence Evaluation

Input: Point clouds $X \in R^{N \times 3}$, $Y \in R^{M \times 3}$ and correspondence $M \in R^{N \times 1}$

Output: Confidence $C \in R^{N \times 1}$ of correspondence M

- 1: $S_{src} \leftarrow \text{KNN}(X, k)$
 - 2: $P_{src} \leftarrow \text{combinations}(S_{src}, 2)$
 - 3: $E_{src} \leftarrow X.\text{reshape}(N, 1, 1, 3).\text{repeat}(1, \frac{(k^2-k)}{2}, 1, 1)$
 - 4: $g_{src} \leftarrow \text{concatenate}(E_{src}, P_{src})$
 - 5: $(l_g^{src}, l_g^{tgt}) \leftarrow \text{GetTri}(g_{src}, g_{tgt})$
 - 6: $L_e \leftarrow \text{sum}((l_g^{src} - l_g^{tgt})^{**2}, \text{dim} = -1) / \text{sum}((l_g^{src} + l_g^{tgt})^{**2}, \text{dim} = -1)$
 - 7: $E_r \leftarrow \text{sum}(\text{sqrt}(\text{Mink}(L_e)), \text{dim} = -1)$
 - 8: $C \leftarrow \psi(2 \times \text{sigmoid}(-\lambda E_r))$
 - 9: **return** C
-

cordance with their contribution in registration, a squeeze-and-excitation (SE) module [23] is adopted. The SE module first extracts a channel descriptor F_{sq} by applying average pooling to the input features F_{in} , then maps F_{sq} to channel weights F_{ex} by means of a neural network, and finally rescales F_{in} with F_{ex} to obtain rescaled features $F_c = F_{ex}F_{in}$.

In summary, by applying the above positional encoding network, Transformer model, and SE module, the feature vectors Φ_X and Φ_Y generated by PFT are defined as

$$\begin{aligned} \Phi_X &= \text{SE}(F_X + \phi(F_Y + P_Y, F_X + P_X)), \\ \Phi_Y &= \text{SE}(F_Y + \phi(F_X + P_X, F_Y + P_Y)). \end{aligned} \quad (8)$$

3.3. Geometric Matching-Based Correspondence Confidence Evaluation

Given features Φ_X and Φ_Y , a set of putative correspondences $M\{x_i, y_j\}$ are established by finding the most similar features $\{\Phi_{xi}, \Phi_{yj}\}$. However, there are outliers in partial-to-partial point cloud registration, which significantly reduces the accuracy. Therefore, the GMCCE module is designed to distinguish between inliers and outliers with a representative descriptor. To accurately describe geometric characteristics, a triangulated descriptor is designed. As shown in Fig. 4, the descriptor employs the side length of triangles to capture geometric characteristics. It offers two advantages: (1) expressing length and angle simultaneously; (2) establishing connections between sampled points.

The GMCCE module is presented in Fig. 2(d), and the detailed procedures are shown in Algorithm 1. First, KNN is used to search for k_s sampled points S_{src} of x_i in src , and then, testing groups g_{src} are obtained by combining S_{src} and x_i ; specifically, each group contains x_i and two points of S_{src} . Afterward, testing groups g_{tgt} are acquired by mapping g_{src} in accordance with the correspondence matrix M . Subsequently, the lengths l_g^{src} and l_g^{tgt} of the triangles constructed by g_{src} and g_{tgt} , respectively, are calculated. Fi-

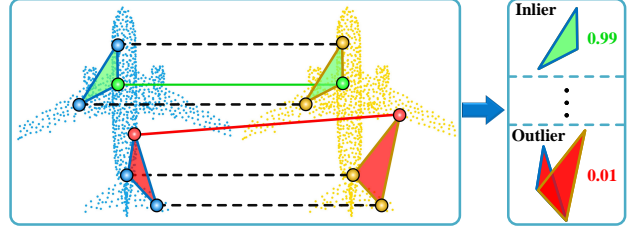


Figure 4. **The demonstration of the triangulated descriptor.** When the correspondence $\{x_i, y_j\}$ is an inlier, the corresponding triangles are similar, and the confidence value $C(x_i, y_j)$ is high. Otherwise, C decreases to a small value if $\{x_i, y_j\}$ is an outlier.

nally, the overall error $E_r(x_i, y_j)$ is calculated by summing the k smallest errors L_e of each group as

$$L_e(g_{src}, g_{tgt}) = \sqrt{\Sigma(l_{g\alpha}^{src} - l_{g\alpha}^{tgt})^2 / \Sigma(l_{g\alpha}^{src} + l_{g\alpha}^{tgt})^2}, \quad (9)$$

$$E_r(x_i, y_j) = \Sigma \text{Mink}([L_e(g_{src}^1, g_{tgt}^1), \dots, L_e(g_{src}^P, g_{tgt}^P)]),$$

where $l_{g\alpha}^{src}$ and $l_{g\alpha}^{tgt}$ denote the side lengths of the triangles constructed by g_{src} and g_{tgt} , respectively; Mink is the operation of taking the k smallest values; P equals $\frac{k(k-1)}{2}$. Then, the confidence $C(x_i, y_j)$ is evaluated as

$$C(x_i, y_j) = \psi(2 \times \text{sigmoid}(-\lambda E_r(x_i, y_j))), \quad (10)$$

where λ is the parameter to adjust the sharpness of the confidence evaluation; ψ is the filter to filter out correspondences with confidence smaller than τ .

3.4. Loss Function

The overall loss function to train our DIT consists of three terms: a transformation loss L_t , a cycle consistency loss L_c , and a discrimination loss L_d . By combining these terms and introducing coefficients α and β to adjust the contribution of each loss term, the final loss function is constructed and defined as

$$L = L_t + \alpha L_c + \beta L_d. \quad (11)$$

Transformation loss: L_t measures the error between the predicted motion R_{XY} , t_{XY} and ground-truth motion R_{XY}^* , t_{XY}^* from X to Y as

$$L_t = \|R_{XY}^T R_{XY}^* - I\|^2 + \|t_{XY}^T t_{XY}^* - I\|^2. \quad (12)$$

Cycle consistency loss: L_c measures the consistency between the predicted motion R_{XY} , t_{XY} from X to Y and R_{YX} , t_{YX} from Y to X as

$$L_c = \|R_{XY}^T R_{YX} - I\|^2 + \|t_{XY} - t_{YX}\|^2. \quad (13)$$

Discrimination loss: L_d measures the discriminative power of extracted features and the accuracy of established correspondences as

$$\begin{aligned} L_d = & -\frac{1}{\|M\|} \sum_{((x_i, y_j) \in M)} [C(i, j) \times \ln S(i, j) \\ & + (1 - C(i, j)) \times \ln(1 - S(i, j))], \end{aligned} \quad (14)$$

where $C(i, j) = 1$ if the correspondence $\{x_i, y_j\}$ is an inlier; otherwise, $C(i, j) = 0$. $S(i, j)$ denotes the similarity between the feature vectors Φ_{x_i} and Φ_{y_j} .

4. Experimental Results

4.1. Experimental Setup

Dataset: The proposed algorithm and baseline methods are evaluated on ModelNet40 [55]. This dataset includes 12,311 meshed computer-aided design (CAD) models in 40 categories, of which 80% are designated for training and the remaining 20% are designated for testing. We randomly sample 1,024 points on the surface of a model as *src* and rescale the points to a unit sphere. An initial rigid transformation is randomly sampled from the following intervals: the rotation along each axis in $[0, 45^\circ]$, and the translation along each axis in $[-0.5, 0.5]$. This initial transformation is then applied to *src* to obtain *tgt*.

Implementation Details: Each LFI layer concatenates the feature vectors from a neighborhood of $k = 20$ and outputs features with 64 dimensions. The MA modules in the PSE and PFT networks each have 4 heads. In the GMCCE module, the parameters $\lambda = 30$, and $k_s = 10$ are obtained by grid search. The network is trained using the Adam [27] optimizer with an initial learning rate of $3e-5$.

Comparison methods: DIT is compared against the representative model-based methods: ICP [4], FGR [65], and FPFH [43] + RANSAC [18] and recent learning-based methods: PointNetLK (PNetLK) [1], DCP [53], DeepGMR [61], IDAM [30], Reagent [3], PNetLK_R [31], and RGM [19]. All experiments are evaluated on an Intel i7-10700 CPU and an RTX 3090 graphics card. ICP, FGR, and FPFH are implemented with the Intel Open3d library [66]. For the other methods, we reproduced the open source code provided by the published papers with the same settings and hyperparameters.

Evaluation metrics: We evaluate the performance of each point cloud registration method using the root mean squared error (RMSE) and the mean absolute error (MAE). All metrics related to rotation are expressed in units of degrees. Comparisons are tested for three scenarios: (1) clean point clouds, (2) low noise partial-to-partial point clouds, (3) high noise partial-to-partial point clouds.

4.2. Matching and Registration Performance

Clean point clouds: We first evaluate the performance on clean point clouds. Qualitative results are shown in Fig. 5(a) and quantitative comparisons are summarized in Table 1. Our method achieves the best performance. Compared with the second-best RGM, our method reduces the rotation and translation errors significantly. The experimental results show that the deep-narrow architecture of the Transformer and the introduction of positional encoding sharpen

Table 1. **Performance on clean point clouds.** The three best results are highlighted in **red**, **green**, **blue**.

Method	Reference	R_{RMSE}	R_{MAE}	t_{RMSE}	t_{MAE}
ICP [4]	SPIE 1992	25.09	14.15	0.157	0.106
FGR [65]	ECCV 2016	10.63	2.335	0.014	0.0045
FPFH [43]	ICRA 2009	15.40	2.643	0.048	0.0090
PNetLK [1]	CVPR 2019	12.02	4.954	0.0064	0.0038
DCP_V2 [53]	CVPR 2019	3.242	2.076	0.0024	0.0015
DeepGMR [61]	ECCV 2020	0.023	0.016	3e-5	2e-5
IDAM [30]	ECCV 2020	1.59	1.109	0.0259	0.018
PNetLK_R [31]	CVPR 2021	1.385	0.120	0.0085	0.0006
Reagent [3]	CVPR 2021	1.073	0.939	0.0023	0.0020
RGM [19]	CVPR 2021	1.8e-4	1.2e-5	2.7e-6	1.6e-7
Ours	-	2.3e-6	1.5e-6	1.7e-8	1.1e-8

the mapping for point cloud alignment. Furthermore, the results verify the ability of the proposed method to identify the structure of the point cloud and the effectiveness in distinguishing between inliers and outliers.

Low noise partial-to-partial point clouds: Partial-to-partial registration is much more challenging due to the existence of outliers and the difficulty of extracting contextual information. Following the similar operation of generating partial-to-partial point clouds in PRNet [54], we remove 200 points from each *src* and *tgt* to obtain a point cloud pair with an overlap rate of approximately 60% (IoU). Then, Gaussian noise sampled from $\mathcal{N}(0, 0.001)$ and clipped to $[-0.001, 0.001]$ is added to each point. The results on low noise partial-to-partial registration are shown in Fig. 5 and Table 2. Our method clearly outperforms the other methods; specifically, the rotation and translation errors are reduced obviously compared with RGM. Due to the lack of information aggregation, the accuracy of DeepGMR and PNetLK_R is much lower than that on clean point clouds. The experimental results verify the importance of aggregating information from the two point clouds and show that DIT can extract contextual information by means of deep information interaction, enabling DIT to precisely identify common structures.

High noise partial-to-partial point clouds: To evaluate the robustness against high noise in partial-to-partial registration tasks, similar to the operation in PRNet [54], Gaussian noise independently sampled from $\mathcal{N}(0, 0.01)$ and clipped to $[-0.05, 0.05]$ is added to each point. The other experimental settings are the same as in the low noise experiment. The results on the high noise partial-to-partial registration are shown in Fig. 5(c) and Table 3. Our method still outperforms other methods; specifically, our method improves the rotation and translation accuracy by 32%–65% compared with RGM. We also note that the accuracy of DCP is reduced by approximately 60% compared with its accuracy in the low noise case. The results reveal that DIT can model global relations, thereby achieving superior

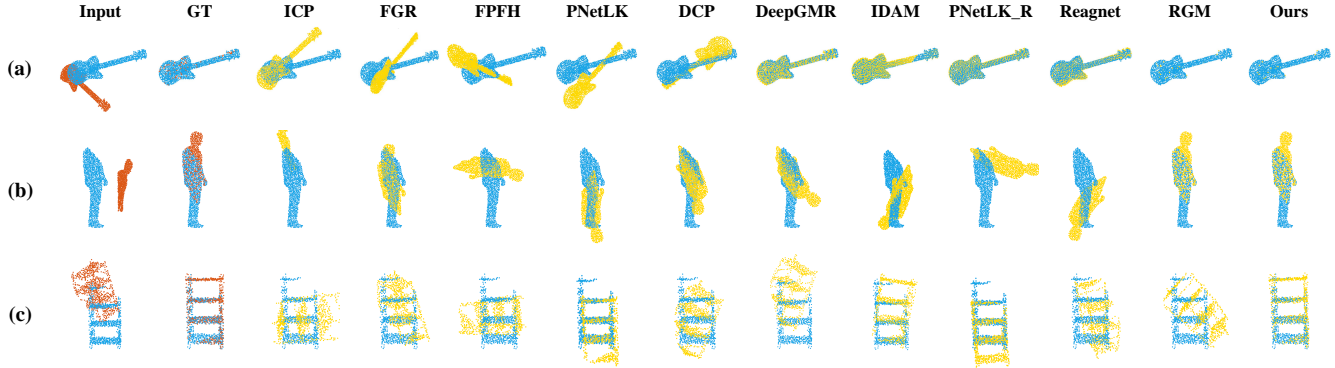


Figure 5. **Qualitative registration results on ModelNet40.** (a) Clean point clouds. (b) Low noise partial-to-partial point clouds. (c) High noise partial-to-partial point clouds.

Table 2. **Performance on low noise partial-to-partial point clouds.** The three best results are highlighted in **red, green, blue.**

Method	Reference	R_{RMSE}	R_{MAE}	t_{RMSE}	t_{MAE}
ICP [4]	SPIE 1992	20.12	11.24	0.13	0.092
FGR [65]	ECCV 2016	21.4	7.03	0.063	0.025
FPFH [43]	ICRA 2009	29.97	8.38	0.083	0.023
PNetLK [1]	CVPR 2019	18.10	12.38	0.131	0.101
DCP_V2 [53]	CVPR 2019	4.43	2.92	0.029	0.022
DeepGMR [61]	ECCV 2020	7.15	4.84	0.13	0.107
IDAM [30]	ECCV 2020	14.44	8.54	0.10	0.07
PNetLK_R [31]	CVPR 2021	7.37	6.32	0.062	0.053
Reagent [3]	CVPR 2021	9.37	8.22	0.055	0.043
RGM [19]	CVPR 2021	0.741	0.099	2.4e-3	8.1e-4
Ours	-	0.014	0.010	6.7e-5	5.3e-5

robustness against high noise.

4.3. Accuracy and Generalization Analysis

To compare the accuracy and generalization, we present the success ratios of all methods in Fig. 6, where the success ratio is defined as the ratio of error (R_{error}, t_{error}) less than the threshold (R_{thres}, t_{thres}). Our method achieves the best performance in all three different settings. With the tightening of convergence thresholds, our method always achieves the highest accuracy and generalization. Fig. 6(a) shows the success ratios on clean point clouds. Due to the strict convergence thresholds, several methods did not converge, only RGM and PNetLK_R are competitive with our method. Our method is clearly the only approach that achieves both the fastest convergence and a success rate of 100%. Specifically, PNetLK_R reaches a 98% success rate, but the error is very large when the matching fails, leading to high MAE and RMSE values in Table 1.

As shown in Fig. 6(b), our method is the only approach with an ultimate success ratio of 99% in both rotation and translation. Only RGM reaches 94%, whereas all the other methods are less than 80%. Compared with the previous experiment, PNetLK_R performs poorly in this partial-to-

Table 3. **Performance on high noise partial-to-partial point clouds.** The three best results are highlighted in **red, green, blue.**

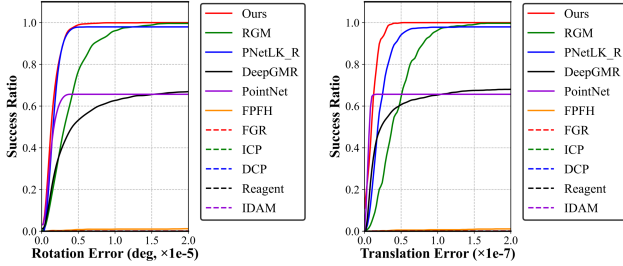
Method	Reference	R_{RMSE}	R_{MAE}	t_{RMSE}	t_{MAE}
ICP [4]	SPIE 1992	20.05	11.33	0.13	0.09
FGR [65]	ECCV 2016	47.58	27.27	0.126	0.088
FPFH [43]	ICRA 2009	55.47	28.9	0.165	0.087
PNetLK [1]	CVPR 2019	18.33	12.17	0.14	0.108
DCP_V2 [53]	CVPR 2019	12.29	7.84	0.097	0.078
DeepGMR [61]	ECCV 2020	8.957	6.243	0.154	0.128
IDAM [30]	ECCV 2020	18.91	11.78	0.093	0.067
PNetLK_R [31]	CVPR 2021	9.837	7.626	0.093	0.075
Reagent [3]	CVPR 2021	11.85	10.47	0.063	0.05
RGM [19]	CVPR 2021	2.068	0.633	0.016	0.0061
Ours	-	1.412	0.357	0.009	0.0021

partial task. The results reveal that the deep-narrow architecture and positional encoding can improve the accuracy on partial-to-partial point clouds. Fig. 6(c) shows the success ratios on the more challenging high noise partial-to-partial point clouds. Our method still surpasses the other methods, achieving a 98% success rate in both rotation and translation. The results demonstrate that modeling global relations strengthens the robustness to high noise, and our full Transformer framework achieves high accuracy and generalization in various registration tasks.

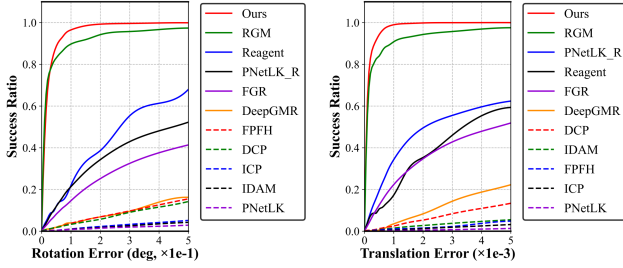
4.4. Ablation Studies

To analyze the effectiveness of the proposed three key components (PSE, PFT, and GMCCE), we present ablation studies by comparing the performance of five variants on the high noise setting. The results of the five variants are shown in Table 4 and Fig. 7.

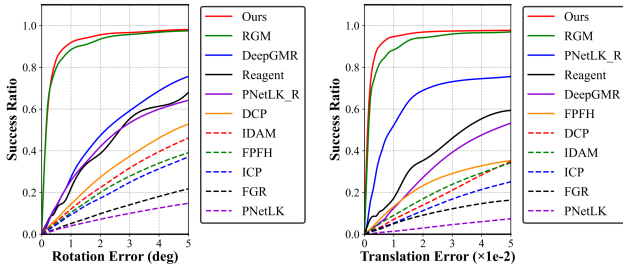
PSE: $DIT_{w/o PSE}$ is designed to exclude the PSE network, the success ratio drops by 93.5%. $DIT_{w/ DGCNN}$ substitutes the PSE module with the DGCNN module [36], and the success ratio drops by 87.2%. The results signify the effectiveness of the PSE network in modeling global relations and identifying structural characteristics.



(a) Clean point clouds



(b) Low noise partial-to-partial point clouds



(c) High noise partial-to-partial point clouds

Figure 6. Accuracy and generalization analysis. The three best results are shown as solid lines in red, green, and blue.

PFT: $DIT_{w/o SW}$ is designed to use a shallow-wide architecture. With this variant, the accuracy declines by 55%–80%, which shows that the deep-narrow architecture establishes more comprehensive associations and facilitates the deep information interaction. $DIT_{w/o PE}$ is designed to exclude the positional encoding network. The results show that the success ratio declines by 39.4%, demonstrating that the positional encoding network enables the Transformer to directly learn the relative position between points, enhancing the robustness to noise.

GMCCE: $DIT_{w/o GMCCE}$ is designed to exclude the GMCCE module. The rotation and translation accuracy drops by 40% – 74%, indicating that GMCCE significantly improves the registration accuracy with the advantage of distinguishing between inliers and outliers.

4.5. Limitations

The experiments have demonstrated the high accuracy and robustness of the DIT on ModelNet40. Since the computational complexity of the attention mechanism is quadratic of the point cloud scale, the application to large-

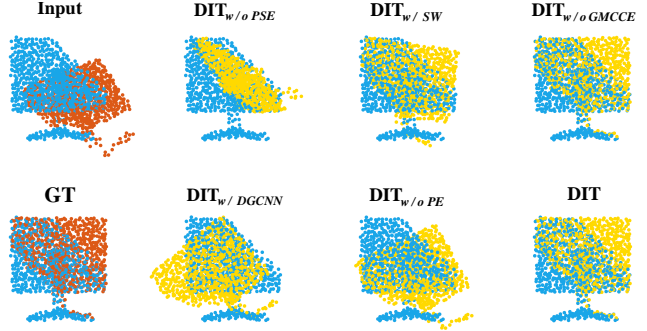


Figure 7. Qualitative ablation results on ModelNet40.

Table 4. Ablation results concerning the effect of PSE, PFT, and GMCCE module. SR denotes the success rate ($R_{thres} = 1, t_{thres} = 0.01$).

Method	R_{RMSE}	R_{MAE}	t_{RMSE}	t_{MAE}	SR
$DIT_{w/o PSE}$	41.84	28.74	0.247	0.197	1.2%
$DIT_{w/o DGCNN}$	18.07	12.19	0.069	0.049	7.5%
$DIT_{w/o SW}$	7.06	1.618	0.020	0.009	71%
$DIT_{w/o PE}$	18.02	6.013	0.091	0.038	55.3%
$DIT_{w/o GMCCE}$	2.36	1.04	0.016	0.008	74.4%
DIT	1.41	0.357	0.009	0.0021	94.7%

scale point clouds requires downsampling or voxelization pre-processing, such operations will reduce the registration accuracy and robustness. Therefore, accurately performing large-scale point cloud registration is a general challenge faced by Transformer-based methods. Several recent methods [11, 52] explored how to improve the efficiency of the attention model, but also caused a certain level of performance degradation.

5. Conclusion

In this work, we explore and propose a novel full Transformer framework DIT for point cloud registration. The DIT effectively models global relations, enhances feature richness, and removes outliers, overcoming the limitations of previous Transformer-based methods. In DIT, PSE is utilized to model dependencies in the entire point cloud and identify the characteristic of neighboring structures, enhancing the robustness to noise. Subsequently, PFT is proposed to improve the discrimination of extracted features by facilitating deep information interaction. Moreover, GMCCE is leveraged to enable accurate alignments by detecting inliers based on geometric consistency. Extensive experiments have been conducted on ModelNet40, exhibiting that our method outperforms previous methods in terms of accuracy, generalization, and robustness. The results demonstrate the potential of the full Transformer framework in point cloud registration tasks. In the future, the application to large scale point clouds will be further investigated.

References

- [1] Yasuhiro Aoki, Hunter Goforth, Rangaprasad Arun Srivatsan, and Simon Lucey. Pointnetlk: Robust & efficient point cloud registration using pointnet. In *Proceedings of the IEEE/CVF Conference on Computer Vision and Pattern Recognition*, pages 7163–7172, 2019. 1, 2, 6, 7
- [2] Jimmy Lei Ba, Jamie Ryan Kiros, and Geoffrey E Hinton. Layer normalization. *arXiv preprint arXiv:1607.06450*, 2016. 4
- [3] Dominik Bauer, Timothy Patten, and Markus Vincze. Reagent: Point cloud registration using imitation and reinforcement learning. In *Proceedings of the IEEE/CVF Conference on Computer Vision and Pattern Recognition*, pages 14586–14594, 2021. 6, 7
- [4] Paul J Besl and Neil D McKay. Method for registration of 3-d shapes. In *Sensor fusion IV: control paradigms and data structures*, volume 1611, pages 586–606. International Society for Optics and Photonics, 1992. 1, 2, 6, 7
- [5] Sofien Bouaziz, Andrea Tagliasacchi, and Mark Pauly. Sparse iterative closest point. In *Computer graphics forum*, volume 32, pages 113–123. Wiley Online Library, 2013. 1, 2
- [6] Tom B Brown, Benjamin Mann, Nick Ryder, Melanie Subbiah, Jared Kaplan, Prafulla Dhariwal, Arvind Neelakantan, Pranav Shyam, Girish Sastry, Amanda Askell, et al. Language models are few-shot learners. *arXiv preprint arXiv:2005.14165*, 2020. 1
- [7] Dylan Campbell and Lars Petersson. Gogma: Globally-optimal gaussian mixture alignment. In *Proceedings of the IEEE conference on computer vision and pattern recognition*, pages 5685–5694, 2016. 2
- [8] Dylan Campbell, Lars Petersson, Laurent Kneip, Hongdong Li, and Stephen Gould. The alignment of the spheres: Globally-optimal spherical mixture alignment for camera pose estimation. In *Proceedings of the IEEE/CVF Conference on Computer Vision and Pattern Recognition*, pages 11796–11806, 2019. 2
- [9] Nicolas Carion, Francisco Massa, Gabriel Synnaeve, Nicolas Usunier, Alexander Kirillov, and Sergey Zagoruyko. End-to-end object detection with transformers. In *European Conference on Computer Vision*, pages 213–229. Springer, 2020. 1
- [10] Dmitry Chetverikov, Dmitry Stepanov, and Pavel Krsek. Robust euclidean alignment of 3d point sets: the trimmed iterative closest point algorithm. *Image and vision computing*, 23(3):299–309, 2005. 1
- [11] Krzysztof Choromanski, Valerii Likhoshesterov, David Dohan, Xingyou Song, Andreea Gane, Tamas Sarlos, Peter Hawkins, Jared Davis, Afroz Mohiuddin, Lukasz Kaiser, et al. Rethinking attention with performers. *arXiv preprint arXiv:2009.14794*, 2020.
- [12] Christopher Choy, Wei Dong, and Vladlen Koltun. Deep global registration. In *Proceedings of the IEEE/CVF conference on computer vision and pattern recognition*, pages 2514–2523, 2020. 1
- [13] Christopher Choy, Jaesik Park, and Vladlen Koltun. Fully convolutional geometric features. In *Proceedings of the IEEE/CVF International Conference on Computer Vision*, pages 8958–8966, 2019. 2
- [14] Jean-Emmanuel Deschaud. Imls-slam: scan-to-model matching based on 3d data. In *2018 IEEE International Conference on Robotics and Automation (ICRA)*, pages 2480–2485. IEEE, 2018. 1
- [15] Jacob Devlin, Ming-Wei Chang, Kenton Lee, and Kristina Toutanova. Bert: Pre-training of deep bidirectional transformers for language understanding. *arXiv preprint arXiv:1810.04805*, 2018. 1
- [16] Alexey Dosovitskiy, Lucas Beyer, Alexander Kolesnikov, Dirk Weissenborn, Xiaohua Zhai, Thomas Unterthiner, Mostafa Dehghani, Matthias Minderer, Georg Heigold, Sylvain Gelly, et al. An image is worth 16x16 words: Transformers for image recognition at scale. *arXiv preprint arXiv:2010.11929*, 2020. 1, 4
- [17] Benjamin Eckart, Kihwan Kim, and Jan Kautz. Hgmr: Hierarchical gaussian mixtures for adaptive 3d registration. In *Proceedings of the European Conference on Computer Vision (ECCV)*, pages 705–721, 2018. 2
- [18] Martin A Fischler and Robert C Bolles. Random sample consensus: a paradigm for model fitting with applications to image analysis and automated cartography. *Communications of the ACM*, 24(6):381–395, 1981. 6
- [19] Kexue Fu, Shaolei Liu, Xiaoyuan Luo, and Manning Wang. Robust point cloud registration framework based on deep graph matching. In *Proceedings of the IEEE/CVF Conference on Computer Vision and Pattern Recognition*, pages 8893–8902, 2021. 1, 3, 6, 7
- [20] Zan Gojcic, Caifa Zhou, Jan D Wegner, Leonidas J Guibas, and Tolga Birdal. Learning multiview 3d point cloud registration. In *Proceedings of the IEEE/CVF conference on computer vision and pattern recognition*, pages 1759–1769, 2020. 1
- [21] Lei Han, Lan Xu, Dmytro Bobkov, Eckehard Steinbach, and Lu Fang. Real-time global registration for globally consistent rgb-d slam. *IEEE Transactions on Robotics*, 35(2):498–508, 2019. 1
- [22] Amir Hertz, Rana Hanocka, Raja Giryes, and Daniel Cohen-Or. Pointgmm: A neural gmm network for point clouds. In *Proceedings of the IEEE/CVF Conference on Computer Vision and Pattern Recognition*, pages 12054–12063, 2020. 1
- [23] Jie Hu, Li Shen, and Gang Sun. Squeeze-and-excitation networks. In *Proceedings of the IEEE conference on computer vision and pattern recognition*, pages 7132–7141, 2018. 5
- [24] Zilong Huang, Xinggang Wang, Lichao Huang, Chang Huang, Yunchao Wei, and Wenyu Liu. Ccnet: Criss-cross attention for semantic segmentation. In *Proceedings of the IEEE/CVF International Conference on Computer Vision*, pages 603–612, 2019. 1
- [25] Gregory Izatt, Hongkai Dai, and Russ Tedrake. Globally optimal object pose estimation in point clouds with mixed-integer programming. In *Robotics Research*, pages 695–710. Springer, 2020. 2
- [26] Bing Jian and Baba C Vemuri. Robust point set registration using gaussian mixture models. *IEEE transactions on*

- pattern analysis and machine intelligence*, 33(8):1633–1645, 2010. 1, 2
- [27] Diederik P Kingma and Jimmy Ba. Adam: A method for stochastic optimization. *arXiv preprint arXiv:1412.6980*, 2014. 6
- [28] Kenji Koide, Masashi Yokozuka, Shuji Oishi, and Atsuhiko Banno. Voxelized gicp for fast and accurate 3d point cloud registration. In *2021 IEEE International Conference on Robotics and Automation (ICRA)*, pages 11054–11059. IEEE, 2021. 1
- [29] Alex Krizhevsky, Ilya Sutskever, and Geoffrey E Hinton. Imagenet classification with deep convolutional neural networks. *Communications of the ACM*, 60(6):84–90, 2017. 1
- [30] Jiahao Li, Changhao Zhang, Ziyao Xu, Hangning Zhou, and Chi Zhang. Iterative distance-aware similarity matrix convolution with mutual-supervised point elimination for efficient point cloud registration. In *Computer Vision–ECCV 2020: 16th European Conference, Glasgow, UK, August 23–28, 2020, Proceedings, Part XXIV 16*, pages 378–394. Springer, 2020. 6, 7
- [31] Xueqian Li, Jhony Kaesemodel Pontes, and Simon Lucey. Pointnettk revisited. In *Proceedings of the IEEE/CVF Conference on Computer Vision and Pattern Recognition*, pages 12763–12772, 2021. 2, 6, 7
- [32] Bruce D Lucas, Takeo Kanade, et al. An iterative image registration technique with an application to stereo vision. Vancouver, British Columbia, 1981. 2
- [33] Haggai Maron, Nadav Dym, Itay Kezurer, Shahar Kovalsky, and Yaron Lipman. Point registration via efficient convex relaxation. *ACM Transactions on Graphics (TOG)*, 35(4):1–12, 2016. 2
- [34] Taewon Min, Eunseok Kim, and Inwook Shim. Geometry guided network for point cloud registration. *IEEE Robotics and Automation Letters*, 2021. 1, 3
- [35] Steven A Parkison, Lu Gan, Maani Ghaffari Jadidi, and Ryan M Eustice. Semantic iterative closest point through expectation-maximization. In *BMVC*, page 280, 2018. 1
- [36] Anh Viet Phan, Minh Le Nguyen, Yen Lam Hoang Nguyen, and Lam Thu Bui. Dgcnn: A convolutional neural network over large-scale labeled graphs. *Neural Networks*, 108:533–543, 2018. 2, 3, 7
- [37] François Pomerleau, Francis Colas, and Roland Siegwart. A review of point cloud registration algorithms for mobile robotics. *Foundations and Trends in Robotics*, 4(1):1–104, 2015. 2
- [38] Charles R Qi, Hao Su, Kaichun Mo, and Leonidas J Guibas. Pointnet: Deep learning on point sets for 3d classification and segmentation. In *Proceedings of the IEEE conference on computer vision and pattern recognition*, pages 652–660, 2017. 2
- [39] Charles R Qi, Li Yi, Hao Su, and Leonidas J Guibas. Pointnet++: Deep hierarchical feature learning on point sets in a metric space. *arXiv preprint arXiv:1706.02413*, 2017. 2
- [40] Prajit Ramachandran, Niki Parmar, Ashish Vaswani, Irwan Bello, Anselm Levskaya, and Jonathon Shlens. Stand-alone self-attention in vision models. *arXiv preprint arXiv:1906.05909*, 2019. 1
- [41] David M Rosen, Luca Carlone, Afonso S Bandeira, and John J Leonard. A certifiably correct algorithm for synchronization over the special euclidean group. In *Algorithmic Foundations of Robotics XII*, pages 64–79. Springer, 2020. 2
- [42] Szymon Rusinkiewicz and Marc Levoy. Efficient variants of the icp algorithm. In *Proceedings third international conference on 3-D digital imaging and modeling*, pages 145–152. IEEE, 2001. 2
- [43] Radu Bogdan Rusu, Nico Blodow, and Michael Beetz. Fast point feature histograms (fpfh) for 3d registration. In *2009 IEEE international conference on robotics and automation*, pages 3212–3217. IEEE, 2009. 1, 2, 6, 7
- [44] Radu Bogdan Rusu, Nico Blodow, Zoltan Csaba Marton, and Michael Beetz. Aligning point cloud views using persistent feature histograms. In *2008 IEEE/RSJ international conference on intelligent robots and systems*, pages 3384–3391. IEEE, 2008. 2
- [45] Samuele Salti, Federico Tombari, and Luigi Di Stefano. Shot: Unique signatures of histograms for surface and texture description. *Computer Vision and Image Understanding*, 125:251–264, 2014. 2
- [46] Aleksandr Segal, Dirk Haehnel, and Sebastian Thrun. Generalized-icp. In *Robotics: science and systems*, volume 2, page 435. Seattle, WA, 2009. 1, 2
- [47] Jacopo Serafin and Giorgio Grisetti. Nipc: Dense normal based point cloud registration. In *2015 IEEE/RSJ International Conference on Intelligent Robots and Systems (IROS)*, pages 742–749. IEEE, 2015. 1
- [48] Chenghao Shi, Xieyuanli Chen, Kaihong Huang, Junhao Xiao, Huimin Lu, and Cyrill Stachniss. Keypoint matching for point cloud registration using multiplex dynamic graph attention networks. *IEEE Robotics and Automation Letters*, 2021. 1, 3
- [49] M Lamine Tazir, Tawsif Gokhool, Paul Checchin, Laurent Malaterre, and Laurent Trassoudaine. Cicp: Cluster iterative closest point for sparse–dense point cloud registration. *Robotics and Autonomous Systems*, 108:66–86, 2018. 1
- [50] Ashish Vaswani, Noam Shazeer, Niki Parmar, Jakob Uszkoreit, Llion Jones, Aidan N Gomez, Łukasz Kaiser, and Illia Polosukhin. Attention is all you need. In *Advances in neural information processing systems*, pages 5998–6008, 2017. 1, 3, 4
- [51] Huiyu Wang, Yukun Zhu, Bradley Green, Hartwig Adam, Alan Yuille, and Liang-Chieh Chen. Axial-deeplab: Stand-alone axial-attention for panoptic segmentation. In *European Conference on Computer Vision*, pages 108–126. Springer, 2020. 1
- [52] Sinong Wang, Belinda Z Li, Madian Khabsa, Han Fang, and Hao Ma. Linformer: Self-attention with linear complexity. *arXiv preprint arXiv:2006.04768*, 2020. 8
- [53] Yue Wang and Justin M Solomon. Deep closest point: Learning representations for point cloud registration. In *Proceedings of the IEEE/CVF International Conference on Computer Vision*, pages 3523–3532, 2019. 1, 3, 6, 7
- [54] Yue Wang and Justin M Solomon. Pnet: Self-supervised learning for partial-to-partial registration. *arXiv preprint arXiv:1910.12240*, 2019. 1, 6

- [55] Zhirong Wu, Shuran Song, Aditya Khosla, Fisher Yu, Linguang Zhang, Xiaoou Tang, and Jianxiong Xiao. 3d shapenets: A deep representation for volumetric shapes. In *Proceedings of the IEEE conference on computer vision and pattern recognition*, pages 1912–1920, 2015. [6](#)
- [56] Heng Yang, Jingnan Shi, and Luca Carlone. Teaser: Fast and certifiable point cloud registration. *IEEE Transactions on Robotics*, 37(2):314–333, 2020. [2](#)
- [57] Jiaolong Yang, Hongdong Li, Dylan Campbell, and Yunde Jia. Go-icp: A globally optimal solution to 3d icp point-set registration. *IEEE transactions on pattern analysis and machine intelligence*, 38(11):2241–2254, 2015. [2](#)
- [58] Zi Jian Yew and Gim Hee Lee. Rpm-net: Robust point matching using learned features. In *Proceedings of the IEEE/CVF conference on computer vision and pattern recognition*, pages 11824–11833, 2020. [2](#)
- [59] Li Yuan, Yunpeng Chen, Tao Wang, Weihao Yu, Yujun Shi, Zihang Jiang, Francis EH Tay, Jiashi Feng, and Shuicheng Yan. Tokens-to-token vit: Training vision transformers from scratch on imagenet. *arXiv preprint arXiv:2101.11986*, 2021. [1](#), [4](#)
- [60] Li Yuan, Qibin Hou, Zihang Jiang, Jiashi Feng, and Shuicheng Yan. Volo: Vision outlooker for visual recognition, 2021. [1](#)
- [61] Wentao Yuan, Benjamin Eckart, Kihwan Kim, Varun Jampani, Dieter Fox, and Jan Kautz. Deepgmr: Learning latent gaussian mixture models for registration. In *European Conference on Computer Vision*, pages 733–750. Springer, 2020. [2](#), [6](#), [7](#)
- [62] Manzil Zaheer, Satwik Kottur, Siamak Ravanbakhsh, Barnabas Poczos, Ruslan Salakhutdinov, and Alexander Smola. Deep sets. *arXiv preprint arXiv:1703.06114*, 2017. [2](#)
- [63] Hengshuang Zhao, Li Jiang, Jiaya Jia, Philip HS Torr, and Vladlen Koltun. Point transformer. In *Proceedings of the IEEE/CVF International Conference on Computer Vision*, pages 16259–16268, 2021. [4](#)
- [64] Hengwang Zhao, Zhidong Liang, Chunxiang Wang, and Ming Yang. Centroidreg: A global-to-local framework for partial point cloud registration. *IEEE Robotics and Automation Letters*, 6(2):2533–2540, 2021. [1](#)
- [65] Qian-Yi Zhou, Jaesik Park, and Vladlen Koltun. Fast global registration. In *European conference on computer vision*, pages 766–782. Springer, 2016. [1](#), [2](#), [6](#), [7](#)
- [66] Qian-Yi Zhou, Jaesik Park, and Vladlen Koltun. Open3d: A modern library for 3d data processing. *arXiv preprint arXiv:1801.09847*, 2018. [6](#)